Behavior of Different-Sized FRP-Confined Square Compound Concrete Columns Containing Recycled Concrete Lumps

G.M. Chen[1], J.J. Zhang[2], Guan Lin, Aff.M.ASCE[3*], Y.F. Wu, M.ASCE[4], T. Jiang[5]

Abstract: A new concrete recycling method is to crush demolished concrete into distinctly large recycled concrete lumps (RCLs), which are in a direct mix with fresh concrete, leading to the so-called compound concrete. Not only can this method decrease the recycling cost by simplifying the recycling process, but it can also increase the recycling ratio. However, existing studies have demonstrated that such compound concrete is inferior to normal concrete. To improve the performance of compound concrete, an effective technique is to confine the compound concrete using fiber reinforced polymer (FRP) confining tubes, as demonstrated by a limited number of studies through tests on circular compound concrete columns. However, no studies have been concerned with FRP-confined compound concrete in rectangular columns. Moreover, the possible column size effect in such columns has never been investigated, although existing studies have revealed that FRP-confined rectangular normal concrete columns of different-sized specimens may exhibit obvious behavioral difference. Against the above background, this paper presents the results of the first-ever experimental program on glass FRP (GFRP)-confined square compound concrete columns of three different sizes. The columns of different sizes had the same effective FRP confinement stiffness and thus the possible column size effect could be revealed. It was observed that the column size effect was not obvious in FRP-confined normal concrete columns in term of compressive strength while it became obvious for FRP-confined compound concrete columns. Finally, three existing compressive strength models originally developed for FRP-confined normal concrete were evaluated using the present test results.

Keywords: Fiber reinforced polymer (FRP); FRP tubes; Recycled concrete lumps (RCLs); Stress-strain behavior; Size effect; Square columns.

[1] Professor, State Key Laboratory of Subtropical Building Science, South China University of Technology, Guangzhou 510641, China. (guangmingchen@scut.edu.cn)
[2] Research Assistant, Department of Civil and Environmental Engineering, The Hong Kong Polytechnic University, Hong Kong, China. (junjie-cee.zhang@connect.polyu.hk)
[3] Research Assistant Professor, Department of Civil and Environmental Engineering, The Hong Kong Polytechnic University, Hong Kong, China. (Corresponding author: guanlin@polyu.edu.hk)
[4] Professor, College of Civil and Transportation Engineering, Shenzhen University, Shenzhen 518060, China. (yufei.wu@szu.edu.cn)
[5] Associate Professor, College of Civil Engineering and Architecture, Zhejiang University, Zhejiang 310058, China. (cetjiang@zju.edu.cn)

Introduction

The recycling of construction waste has raised concerns for decades. A typical concrete recycling method is to crush demolished concrete into recycled aggregates (RAs) for making new concrete. Such concrete with all or partial aggregates replaced by RAs is referred to as recycled aggregate concrete (RAC). Existing studies on RAC have concluded that RAC generally performs inferior to its natural aggregate concrete (NAC) counterpart, especially with a large replacement ratio of RAs (Ajdukiewicz and Kliszczewicz 2002; Poon et al. 2004; Topcu and Sengel 2004; Xiao et al. 2005; Rahal 2007; Rao et al. 2011; Xiao et al. 2014; Kou and Poon 2015; Li et al. 2015; Medina et al. 2015; Deresa et al. 2020; Chen et al. 2021). As a result, the use of RAC has so far been limited to nonstructural components, such as road bases, paving blocks, and landfills (Poon and Chan 2006a, b). In addition to its inferior performance, the production of RAs involves complicated and time-consuming recycling processes, including crushing, screening, and washing. The associated large energy consumption and potential unfavorable impact on environment in producing RAs are also increasingly becoming new concerns of the industry and research communities.

Wu et al. (2008) proposed a new method by crushing demolished concrete into distinctly large recycled concrete lumps (RCLs) for a direct mix with fresh concrete (FC) to produce the so-called compound concrete (Teng et al. 2016). Compared with traditional recycling methods, this novel recycling method has many advantages such as: (1) it significantly decreases the recycling costs by simplifying the manufacturing process; and (2) it increases the recycling ratio (the weight ratio between the recycled portion and the total old concrete) as the mortar in the RCLs can also be reused in the new concrete. Numerous studies have been carried out by Wu's research group to demonstrate the feasibility of this novel recycling method. Specimens made of compound concrete have been tested under: (1) axial compression (Wu et al. 2011b; Wu et al. 2013a; Wu et al. 2014; Wu et al. 2015); (2) bending (Wu et al. 2011a); (3) shear (Wu et al. 2011a); and (4) cyclic loading (Wu et al. 2012; Wu et al. 2013b). Particularly, compound concrete-filled steel tubes (CCFSTs) under various loading conditions have been investigated (Wu et al. 2012; Wu et al. 2013b; Zhao et al. 2016; Wu et al. 2018; Zhao et al. 2020) and such structural component has been used in practice (Wu et al. 2011b).

However, much more research is still needed to promote the use of RCLs as existing studies have shown that compound concrete performs inferior to normal concrete when the RCLs are weaker than the FC, which is common in practice. The inferior performance of compound concrete is attributable to at least the following aspects: (1) compound concrete is in a much more heterogeneous property than normal concrete due to the presence of RCLs, particularly when the difference in strength between FC and RCLs is relatively large; and (2) weaknesses exist at the interfaces between FC and RCLs. It has been found that the strength of compound concrete reduces as the mix ratio of RCLs (the ratio between the weight of RCLs and that of the total compound concrete) increases; the strength of compound concrete also decreases as the strength difference between FC and RCLs increases in the case that the mix ratio of RCLs remains the same and the RCLs are weaker than the FC (Wu et al. 2015). Some other drawbacks of compound concrete also limit its wide application, especially in steel reinforced concrete members, including: (1) the difficulty of achieving a high RCL mix ratio due to the presence of steel reinforcement (Wu et al. 2012); (2) the potential inferior bond behavior between steel reinforcement and compound concrete due to the adverse effects of RCLs, which is similar to the situation in RAC (Ajdukiewicz and Kliszczewicz 2002; Xiao and Falkner 2007); (3) the potential corrosion of internal steel reinforcement caused by premature cracking in compound concrete due to the weaknesses of the interfaces between FC and RCLs.

To enhance the properties of compound concrete, Teng et al. (2016) proposed the concept of using fiber reinforced polymer (FRP) confining tubes to confine compound concrete to form the so-called FRP-confined compound concrete (FCCC) columns. Their test results revealed that, with the confinement from the filament wound glass FRP (GFRP) tube, both the compressive strength and the ductility of compound concrete were improved to be close to those of the FC. Zhou et al. (2021a) carried out an experimental study on compound concrete columns confined with carbon FRP (CFRP) tubes which were prefabricated using the wet lay-up method. Their findings were generally in consistent with those of Teng et al. (2016). Both studies revealed that, through the provision of a sufficiently large FRP confinement, most of the aforementioned weaknesses of compound concrete due to the presence of RCLs could be minimized. More recently, Zhou et al. (2021b) conducted cyclic compression tests on FCCC columns confined with filament wound GFRP tubes and found that the cyclic stress-strain behavior of FRP-confined concrete was little affected by the presence of RCLs.

However, the above studies (Teng et al. 2016; Zhou et al. 2021a, b) were concerned only with circular FCCC columns. No studies have been conducted on rectangular or square FCCC columns despite that they are commonly found in practice. Existing studies have shown that FRP confinement in rectangular columns is non-uniform and compared with circular columns, the FRP confinement in rectangular columns is much less effective (Lam and Teng 2003; Lim and Ozbakkaloglu 2014; Lin and Teng 2020). Due to at least the above reasons, it have been revealed that FRP-confined rectangular normal columns of different sizes often exhibit significantly different compressive behaviors (i.e., the column size effect) (Matthys et al. 2005; Rocca 2007; De Luca et al. 2011; Wang et al. 2016; Zeng et al. 2018). Thus, the column size effect may also exist in rectangular FCCC columns. However, due to the presence of RCLs and the weaknesses at the interfaces between RCLs and FC, the column size effect in rectangular FCCC columns may become much more complicated, which needs an urgent investigation before the safe and confident use of compound concrete in practice.

Against the above background, the present study aims at exploring the column size effect in square FCCC columns through the first-ever experimental program on such columns subjected to axial compression. Square column specimens with three sizes (sectional width = 200, 300 and 400 mm) were tested. The different-sized column specimens had the same effective FRP confinement stiffness, so that the column size was the only test variable. In addition, the effects of RCL characteristic size ratio (the ratio of the characteristic size of RCLs and the sectional width; the RCL characteristic size is defined to be the maximum sieve size that the RCLs can pass through) and the FRP tube thickness were examined in detail. Finally, three existing compressive strength models originally developed for FRP-confined normal concrete were evaluated using the present test results.

Experimental Program

Specimen design

A total of 20 square concrete column specimens of three different sizes (sectional width b = 200, 300, and 400 mm, excluding the FRP tube thickness) were prepared. The specimens were classified into three different groups according to their sizes (namely, Groups 1, 2 and 3 for 200-, 300-, and 400-mm-width specimens, respectively). The specimens of different sizes were geometrically proportional in all aspects (Fig. 1), including the column height H, sectional width b, thickness of FRP tube t_f, and FRP overlapping length. The mix ratio of RCLs of all compound concrete specimens was fixed to 0.33 as suggested by Zhao et al. (2016) for the ease of casting compound concrete in practice. The different-sized FRP-confined concrete specimens possessed the same effective FRP confinement stiffness [calculated by $2E_f t_f/D$, where E_f = FRP tube hoop elastic modulus; t_f = FRP tube thickness; and $D = \sqrt{2}b$ which is the diameter of the equivalent circular section (Lam and Teng 2003)]. All the specimens had the same corner radius ($2r_c/b$) of 0.3. Besides, Group 1 included one specimen confined with a 1-layer FRP tube and Group 3 included one specimen confined with a 2-layer FRP tube to study the effect of FRP tube thickness (see Table 1). The ranges of RCL characteristic size ratios, β, (the ratio of RCL characteristic size, d, and the section width, b) of different-sized specimens were kept the same (i.e., β = 0, 0.25-0.33, or 0.33-0.5).

The details of all the test specimens are listed in Table 1. Each column specimen is identified by a notation which starts with "S" denoting a square column specimen, followed by the number 200/300/400 denoting the column sectional width. This is then followed by "L" and a digit number indicating the layer number of the FRP tube and letter "G" plus 1 or 2 (for compound concrete specimens) indicating the RCL characteristic size ratio range of 0.25-0.33 or 0.33-0.5.

Material properties

Recycled concrete lumps (RCLs)

The RCLs of desired sizes were crushed from demolished concrete collected from a local building demolition site using pneumatic pick hammers. The RCLs were divided into six types according to their characteristic sizes (i.e., 50-67 mm, 67-100 mm, 75-100 mm, 100-133 mm, 100-150 mm, and 133-200 mm, respectively) (Fig. 2). The mix ratio of RCLs was kept the same (η = 0.33) for all the column specimens (Table 1). The strength of the RCLs was obtained by compressing fifteen cylindrical core samples (diameter = 100 mm; height = 100 mm) which were drilled from the demolished concrete. The average strength of RCLs was measured to be 35.8 MPa. As per the Chinese standard CECS03-2007 (CECS 2007), a cylindrical core sample of such dimensions generally has a compressive strength similar to that of a 150-mm-length concrete cube; the latter was used to obtain the compressive strength of FC as discussed later. The physical properties of RCLs, including the crushing value [17.8%, according to JGJ 52 (2006)] and the Los Angeles abrasion (LAA) value [34.5%, according to JTG E42 (2005)] were also tested.

Fresh concrete (FC)

The same batch of ready-mix concrete, which was provided by a local concrete supplier, was used as the FC for all the column specimens. Crushed granite aggregate with a nominal dimension of 16-31.5 mm was used. Three standard concrete cylinders (150 mm × 300 mm) and three 150-mm-length cubes were prepared using the FC and compressed to obtain the properties of the FC. The cubes were tested for the compressive strength only and thus a load control mode (loading rate = 0.3 MPa/s) was adopted, while a displacement control mode (displacement rate = 0.18 mm/min) was adopted for testing the cylinders according to ASTM C469 (2014). The average 28-Day strengths obtained from the concrete cube tests and the cylinder tests were 69.4 MPa and 58.9 MPa, respectively. It can be seen that the strength of FC was much higher than that of RCLs, which is reasonable as old structures with a low concrete strength are generally used to produce RCLs in practice. However, it should be noted that, in the current practical application of RCLs, the strength difference between FC and RCLs should be limited to a particular value to avoid any detrimental effects on the behavior of compound concrete. Such a limit value may become larger or even be ignored in the future when the effects of strength difference on the stress-strain behavior of compound concrete have been deeply understood.

GFRP tubes

The GFRP tubes in the present study were prefabricated manually using the common wet lay-up process in which resin impregnated glass fiber sheets were continuously wrapped around a square wooden mold (see Fig. 3). The fibers were running in the tube hoop direction only. Before the fiber wrapping, a thin plastic film was attached around the mold to ensure a smooth external surface of the mold and thus an easy demolding process for the GFRP tubes. The fiber wrapping initiated at one of the rounded corner edges on a flat side surface (covering the entire area of the flat side) and terminated at the centerline of the same flat side, and thus the overlapping length was $(b/2 - r_c)$ for all the specimens. An additional GFRP strip with a width of 1/10 of the tube height was wrapped around each tube end to avoid unexpected end failure (Fig. 3). The tubes were cured for at least 48 hours in the laboratory before demolding. Three 1-layer GFRP flat coupons were tensioned to rupture as per ASTM D3039 (2017) to obtain the GFRP tube properties in the hoop direction. The average tensile strength, elastic modulus and rupture strain were obtained to be 1,410 MPa, 75 GPa, and 1.87%, respectively (nominal fiber thickness per layer = 0.36 mm) (Table 2). As the FRP tubes possessed fibers only in the tube hoop direction, the axial stiffnesses of these tubes were negligibly small, which means that the FRP tubes served mainly to confine the inner concrete. However, in practice, filament wound FRP tubes with significant axial stiffness are still more desirable to be used. In the present paper, compound concrete columns confined with any type of FRP tube are collectively referred to as FCCC columns unless otherwise specified.

Preparation of specimens

All the RCLs were fully watered to a saturated state and then dried using a dry cloth glove (i.e., a saturated surface-dry condition) before mix with FC. Before concrete casting, the FRP tubes were fixed on flat wooden plates with water-proof sealant. The GFRP tubes directly served as molds for concrete casting of confined specimens, while wooden molds were used for unconfined specimens. For casting the specimens containing RCLs, a layer of FC of approximately 20 mm thick was poured into the FRP tube or mold first, followed by the alternate pouring of RCLs and FC. The compactness of the concrete was ensured by inserting a vibrating poker into the concrete during the casting process (Fig. 4). The unconfined specimens were de-molded from the wooden molds after being cured for 24 hours. All the column specimens covered with plastic films were cured for at least 28 days in the laboratory before compression tests. High-strength gypsum was used to cap each of the two ends of the specimens to ensure uniform axial loading.

Test set-up and instrumentation

Six LVDTs (linear variable displacement transducers) were used to capture the axial shortenings of each specimen. Among them, four were installed at the four flat sides covering 1/3 of the specimen height and two were attached on the loading plates at the bottom to capture the total axial shortenings (Fig. 5a) (note that the loading was processed by moving the bottom loading plate upwards). Four axial strain gauges (SGs) and sixteen hoop SGs were installed on the FRP tube at the mid-height of each FRP-confined specimen; the gauge length was 20 mm for the 300- and 400-mm-width column specimens and 10 mm for the 200-mm-width column specimens. The four axial SGs were installed at the four flat side centers; the sixteen hoop SGs were installed around the circumference of the section at the mid-height. Among the sixteen hoop SGs, four were installed at the corner centers, another four were installed at the flat side centers, and the remaining eight were installed near the points with curvature discontinuity (i.e., transition points between the corners and the flat sides) (Fig. 5b). For each unconfined specimen, two 100-mm axial SGs and two 50-mm hoop SGs were installed at the flat side centers. All the specimens were tested between two end loading plates on a 15,000-kN capacity testing machine (Fig. 5c). A displacement control mode with a rate of 0.36 mm/min was used for all the specimens (ASTM C469 2014; Zhang et al. 2017). All data, including the strains, displacements, and loads were simultaneously recorded by a data logger. It should be noted that the load was applied directly on the entire column cross-section (i.e., concrete and FRP tube) through the end loading plates. This loading condition is common for the new construction of a concrete filled FRP tubular column in which the FRP tube is used as the permanent formwork for casting concrete. Note that the FRP tubes used in this study were fabricated via the wet lay-up method with fibers running in the tube hoop direction only and thus they had negligibly small axial stiffnesses. As a result, the applied axial load was resisted mostly by concrete. However, if an FRP tube with a significantly large axial stiffness (e.g., a filament wound FRP tube) is used, the axial load resisted by the tube may be large and could not be ignored (Xie et al. 2020).

Test Results and Discussions

Failure modes

Fig. 6 shows the failure modes of the column specimens after test. Concrete crushing with huge cracks was observed for all the unconfined specimens. The specimens without RCLs failed suddenly and seriously due to the brittleness of high-strength FC, while the specimens containing RCLs appeared to fail more gradually because of the much lower compressive strength of compound concrete. Fig. 7 shows a close-up view of two typical unconfined specimens containing RCLs after the test. It can be seen that the RCLs and FC were well bonded together and the major cracks went through the RCLs rather than along the interfaces between RCLs and FC. This observation may be partially attributable to the use of FC with a much higher strength than RCLs. However, other failure modes (e.g., major cracks going around the interfaces between RCLs and FC) may occur if RCLs with a larger compressive strength are used. Most of the FRP-confined concrete column specimens failed by a sudden FRP tube rupture in the hoop direction (Fig. 6). As the loading processed, white patches on the FRP tube first appeared when the strength of unconfined concrete was approximately reached, implying resin damage in the tube. As the deformation increased, the regions of the white patches expanded with continuous snapping sounds of fiber rupture. Finally, the tube failed with a major fiber rupture with an explosive sound. The rupture of FRP generally occurred near one of the corners, which is in consistency with the observations on FRP-confined rectangular concrete columns (e.g., Wang et al. 2012b; Zeng et al. 2018; Lin and Teng 2020). It seems that the failure modes of the test specimens were not affected by the column size or the presence of RCLs.

Axial stress-axial strain curves

Figure 8 shows the axial stress-axial strain curves of concrete in all the test column specimens. The axial stresses were calculated from the applied axial loads of the column specimen divided by the cross-sectional area of concrete. The axial loads resisted by the GFRP tubes were ignored as a result of the negligible tube axial stiffness. The four mid-height LVDTs were adopted to obtain the axial strains (see Fig. 5). The key test results of the column specimens are summarized in Table 3, including the peak axial stress (compressive strength) (f'_{cc}), the corresponding axial strain (ε_{cc}), the axial stress and strain at FRP rupture ($f'_{cu,r}$ and $\varepsilon_{cu,r}$), and the ultimate axial strain (ε_{cu}) corresponding to FRP rupture or an 15% reduction in axial stress after the peak, whichever occurs first.

Figure 8a shows the axial stress-axial strain curves of unconfined concrete column specimens with different RCL characteristic size ratios and different sizes. It is evident that the stress-strain behavior of unconfined concrete is dramatically influenced by the presence of RCLs. More specifically, the following observations can be made from Fig. 8a: (1) the peak axial stresses of specimens with RCLs are evidently smaller than those of the specimens without RCLs; (2) the peak axial stress decreases noticeably as the RCL characteristic size ratio increases, indicating that larger RCLs lead to a more negative effect on the response of compound concrete; (3) due to the reduced peak axial stress, the axial strains at peak stress (ε_{cc}) of specimens containing RCLs are generally smaller than those without RCLs. The above observations on unconfined compound concrete are generally consistent with those observed by other researchers (e.g., Wu et al. 2013a; Wu et al. 2014; Wu et al. 2015; Teng et al. 2016; Zhou et al. 2021). Note that the RCLs in the present study had a smaller compressive strength than the FC, which is the main reason that the strength of compound concrete is dramatically reduced by RCLs. However, if RCLs with a higher strength are used, the compound concrete may exhibit a higher strength than the FC (Teng et al. 2016).

Figure 8b provides the axial stress-axial strain curves of all test FRP-confined specimens with different RCL characteristic size ratios and different sizes. The curves of specimens without RCLs (i.e., specimens S200L2, S300L3 and S400L4) exhibit a sudden drop in stress after the peak, which indicates that the confinement from the FRP tubes was not large enough to cause a commonly seen monotonically increasing bilinear axial stress-axial strain curve (i.e., a hardening stress-strain behavior). After the sudden stress drop, the axial stress increased rapidly and then remained in a stable stress level until the FRP rupture. Although the specimens were confined with a relatively weak FRP confinement, the compressive strength of the FRP-confined specimens are significantly larger than those of the corresponding unconfined specimens (Fig. 8a), which is still desirable in practice. Nevertheless, the investigation of columns with stronger FRP confinement should be carried out in the future. For the FRP-confined compound concrete specimens, the compressive strengths are remarkably smaller than those of the corresponding FRP-confined specimens without RCLs (Fig. 8b). However, the post-peak axial stress reduces much more gradually in specimens containing RCLs and there were no sudden axial stress drops after the peak stress in these specimens. This observation is different from those of some previous studies which showed that the presence of RCLs did not affect obviously the stress-strain behavior of FRP-confined concrete (Zhao et al. 2016; Zhou et al. 2021a). The major difference between the present study and the previous studies is that the specimens in previous studies had a sufficiently strong FRP confinement which resulted in a hardening stress-strain behavior for the specimens, while the FRP confinement of the present test column specimens was insufficient to ensure a hardening behavior as shown in Figs. 8b and 8c. It may thus be concluded that the negative effect caused by RCLs could be eliminated only if the compound concrete is under sufficiently large FRP confinement. However, more research is needed in the future to deeply understand this observation.

Compared with the corresponding unconfined compound concrete column specimens (Fig. 8a), both the compressive strength and the ductility (see discussions in Section "Ductility index") of FRP-confined compound concrete specimens are obviously enhanced. Fig. 8b also shows that, for the same RCL mix ratio (η = 0.33), larger RCLs (i.e., a larger RCL characteristic size ratio) led to lower compressive strength of FRP-confined compound concrete for the 200- and 300-mm-width specimens. However, for the 400-mm-width specimens, the size of RCLs did not seem to significantly affect the stress-strain curve shape, while the ultimate axial strain of the specimen with larger RCLs (S400L4G2) is much smaller. More research, however, is needed in the future to allow more conclusive observations on the effect of RCL size to be made since only a single specimen was tested for each column parameter in the present study.

Figure 8c shows the stress-strain curves of FRP-confined compound concrete specimens with different FRP tube thicknesses but the same RCL characteristic size ratio of 0.33-0.50. As expected, the specimens with a larger FRP tube thickness perform significantly better in terms of both strength and ductility.

Effect of column size

To examine the possible column size effect, the axial stress-axial strain curves of column specimens with the same effective FRP confinement stiffness and RCL characteristic size ratio but different sizes are shown in Fig. 9. It can be observed from Fig. 9a that the column size has only a small influence on the axial stress-axial strain curve (including the initial axial stiffness) of unconfined specimens without RCLs although the peak stress of the small-scale specimen is slightly larger than those of the specimens of larger sizes. However, for the specimens containing RCLs (with RCL characteristic size ratios of both 0.25-0.33 and 0.33-0.50), the curves of specimens of different column sizes are significantly different from each other in terms of both the peak stress and the curve shape. The peak axial stress and the initial axial stiffness decrease dramatically with an increase in the column size.

Figure 9b shows the axial stress-axial strain curves of all the FRP-confined column specimens. The curves of specimens of the same FRP confinement stiffness and RCL characteristic size ratio but different sizes are shown in each sub-figure. It can be seen that the effect of column size is not obvious on the compressive strength of FRP-confined specimens without RCLs although their corresponding strains seem significantly different. Note that these specimens exhibited a sudden load drop near the peak load, which casts doubt on the reliability of the measured strains near and after the peak stress. For FRP-confined specimens with RCL characteristic size ratios of 0.25-0.33, the stress-strain curves exhibit a remarkable column size effect with a larger column performing inferior to (in terms of both the peak stress and initial axial stiffness) a smaller column. However, when the RCL characteristic size ratio becomes larger, the column size effect becomes less significant partially due to the greatly reduced compressive strength with the use of larger RCLs. This also applies to the specimens with a lower FRP confinement stiffness (S200L1G2 and S400L2G2) (Fig. 9b).

It can be noted that the difference in the axial stress-axial strain curves of different-sized specimens in Fig. 9b stems from at least two sources: (1) the size effect in unconfined concrete specimens (Fig. 8a); and (2) the effect of RCL on the strength of unconfined compound concrete (Fig. 8a). To eliminate the above two factors, the axial stresses and strains in Fig. 9b are normalized by the compressive strength (f'_{cco}) and the axial strain (ε_{cco}) of the corresponding unconfined concrete specimens (with the same column size and RCL characteristic size ratio) and the normalized axial stress-axial strain curves are plotted in Fig. 10. For the specimens without RCLs, the normalized axial stress-axial strain curves exclude the size effect of the corresponding unconfined column specimens, although the size effect is not significant as shown in Fig. 9a. The normalized curves of specimens S200L2 and S400L4 are almost identical to each other before the peak stress; specimen S300L3, however, has much larger normalized axial strains as discussed earlier. For the specimens with RCL characteristic size ratios of 0.25-

0.33 (S200L2G1, S300L3G1 and S400L4G1), the normalized curves of different-sized specimens start to deviate from each other near the peak axial stresses. The normalized peak stress of the 400-mm-width specimen is the smallest; however, the normalized peak axial stress of specimen S300L3G1 is unexpectedly larger than that of specimen S200L2G1. For the specimens with RCL characteristic size ratios of 0.33-0.50 (S200L2G2, S300L3G2 and S400L4G2), the normalized peak axial stress increases as the sectional width increases. The same phenomenon also applies to the two-sized specimens with lower FRP confinement stiffness (S200L1G2 and S400L2G2). The above observations suggest that, after the effects of column size and RCLs on the corresponding unconfined concrete strength are eliminated, the size effect of FRP-confined compound concrete columns is not obvious. Note that existing findings on column size effect have revealed that a larger-scale column specimen generally behaves inferior to a smaller-scale specimen (e.g., Bažant and Kwon 1994; Wang et al. 2016).

Figure 11 shows the variations of the compressive strength with the column sectional width for the specimens with three different RCL characteristic size ratios. It is evident that the strength decreases obviously with the increase in the sectional width for the unconfined column specimens containing RCLs (Fig. 11a); however, the size effect is not obvious for specimens without RCLs (Fig. 11a), which is consistent with the observations made from Figs. 8-10. A similar trend can be seen from Fig. 11b for the FRP-confined concrete specimens. Besides, it is clear that, for both unconfined and confined column specimens, the negative effect of RCLs on the concrete compressive strength is remarkable and a larger RCL characteristic size ratio generally leads to a larger decrease in strength (Figs. 11a and 11b). The amplified size effect due to the existence of RCLs is believed to be caused by the inferior properties of the interfacial transition zones (ITZs) between RCLs and FC, which may introduce microcracks or weaknesses in compound concrete; besides, the existing microcracks/damage in RCLs caused during the producing of RCLs or in the service life of old concrete (from which RCLs are produced) play a role similar to that of the weak ITZs. It can also be seen that the column size effect is slightly more obvious for the unconfined specimens with a larger RCL characteristic size ratio (Fig. 11a) due to the increased microcracks or weakness in the compound concrete. Such microcracks or weakness forms as a major source for the concrete size effect (Bažant 2000). For FRP-confined concrete column specimens (Fig. 11b), however, the use of a larger RCL characteristic size seems to reduce the column size effect, partially due to the significantly lower strength of compound concrete with a larger RCL characteristic size which resulted in more effective FRP confinement. However, experimental data with more detailed observations are needed for more solid conclusions to be drawn in the future. Figure 11c shows the variations of the normalized strength with the column sectional width. In consistency with the observations from Fig. 10b, the size effect is not obvious after the size effect of the corresponding unconfined concrete column and the effect of RCLs on the strength of unconfined concrete are both taken into consideration.

It should be noted that the above observations may not be sufficiently conclusive for FRP-confined compound concrete in square columns, as only one single specimen was tested for each column parameter. More specimens and more than one nominally identical specimens should be tested in future studies for more conclusive observations on the column size effect to be made.

Ductility index

The ductility index (DI) is defined as the axial strain ratio of the ultimate strain (ε_{cu}) and the yield strain (ε_y) in the present study. The ultimate strain (ε_{cu}) corresponds to the rupture of FRP tube or a 15% reduction in axial stress after the peak, whichever occurs first. The yield strain (ε_y) is defined according to the equal energy method (Park 1988). Table 3 lists the DI values for all the test FRP-confined concrete specimens. The ductility indices of the specimens containing RCLs are obviously larger than their counterparts without RCLs, which is in consistency with the curves in Fig. 8b. For the 300- and 400-mm-width specimens, the DI values of specimens with an RCL characteristic size ratio of 0.25-0.33 [S300L3G1 (3.01) and S400L4G1 (3.02)] are larger than those with an RCL characteristic size ratio of 0.33-0.50 [S300L3G2 (2.69) and S400L4G2 (2.07)] while a reverse trend is shown for the small-scale specimens [S200L2G1 (2.10) versus S200L2G2 (3.19)]. The reverse trend in the small-scale specimens was due to the fact that the ultimate axial strain of specimen S200L2G1 corresponded to a 15% reduction in axial stress after the peak while the remaining specimens had ultimate axial strains corresponding to FRP rupture (Table 3).

FRP hoop strains

The strain gauges at three different locations at the mid-height section (Fig. 5b) were used to obtain the FRP hoop strains: the corner centers ($\varepsilon_{h,c}$); the centers of flat sides ($\varepsilon_{h,f}$); and the transition points ($\varepsilon_{h,t}$). The average FRP hoop strains at these locations corresponding to peak axial stress (f'_{cc}) and FRP rupture ($f'_{cu,r}$) are listed in Table 4 (the hoop strain gauges installed in the overlapping zones were excluded). The average value obtained from four (at the corner or flat side centers) or seven (at the transition points, excluding the strain gauge in the overlapping zone) strain gauges for each location was reported in the table. The maximum FRP hoop strain ($\varepsilon_{h,max}$) and its associated strain gauge recorded for each FRP-confined specimen during the loading process are also provided in the table. Fig. 12 shows the FRP hoop strain ratios [i.e., the ratio of the FRP hoop rupture strain measured in the column test and the FRP rupture strain obtained from flat coupon tests (1.87%)] recorded at the three different locations versus the sectional width. It is seen that the FRP hoop strains at the flat side centers are generally larger than those at the corner centers and the transition points, which is in consistency with the observations for FRP-confined rectangular columns (e.g., Wang et al. 2012b; Zeng et al. 2018; Zhu et al. 2020). The effects of column size and RCL characteristic size ratio on the FRP hoop strain seem to be limited. Fig. 12d shows that the maximum FRP hoop strain ratios of the test column specimens at FRP rupture were around 0.6, which is close to the value (0.624) reported by Lam and Teng (2003) for GFRP-confined circular normal concrete columns.

Comparison with Existing Strength Models

Numerous stress-strain models have been proposed for FRP-confined concrete in rectangular columns (e.g., Lam and Teng 2003; Wang et al. 2012a; Wei and Wu 2012; Lim and Ozbakkaloglu 2014; Fanaradelli et al. 2019; Jiang et al. 2019; Li et al. 2019). The models of Wang et al. (2012a), Wei and Wu (2012) and Lin (2016) which are typical strength models applicable to FRP-confined concrete with a softening stress-strain behavior are evaluated in this section. Wang et al.'s (2012a) model and Wei and Wu's (2012) model employ the FRP rupture strain from coupon tests in calculating the strength of confined concrete with a softening behavior; however, Lin's (2016) model adopts the effective FRP confinement stiffness in calculating the compressive strength. It is known that the strength of FRP-confined concrete with a softening behavior is reached before FRP rupture and thus it may be more rational in concept that the strength is not directly related to the FRP rupture strain for such softening confined concrete. For the detailed equations of the three models, the readers are referred to the original sources.

In making predictions for the strength of FRP-confined concrete, the strengths of unconfined concrete obtained from small-scale standard concrete cylinders or large-scale column specimens are commonly used (Lin et al. 2016). As the presence of RCLs dramatically reduces the strength of compound concrete (see Fig. 8a), the strength of unconfined compound concrete should be obtained from specimens containing RCLs. In addition, the effect of RCL characteristic size ratio on the strength of unconfined compound concrete should also be considered when evaluating the compressive strength of FRP-confined compound concrete. Therefore, the strength of unconfined compound concrete obtained from the small-scale unconfined specimens (referred to as the unconfined compound concrete strength, f_c', obtained from small-scale specimens) could be used to predict the compressive strengths of FRP-confined compound concrete specimens with the same RCL characteristic size ratio. However, it is obvious that this strength, f_c', did not include the column size effect (for medium- and large-scale specimens). To include the column size effect, the strength of unconfined compound concrete obtained from the specimen with the same size (and also the same RCL characteristic size ratio) as the FRP-confined compound concrete specimen should be used (referred to as the strength of the control unconfined compound concrete column, f_{cco}'). Note that f_c' is identical to f_{cco}' for the small-scale specimens. Table 3 lists the two strengths of unconfined compound concrete (f_c' and f_{cco}') for each FRP-confined specimen. In the evaluation of the three existing strength models, both strengths (f_c' and f_{cco}') were evaluated in making the predictions.

Figures 13a and 13b show the performance of the three strength models in predicting the compressive strengths of the test FRP-confined compound concrete columns. For the specimens without RCLs ($\beta = 0$), when the strength of f_c' was used, both models of Lin (2016) and Wang et al. (2012a) predict the test results reasonably well, while the model of Wei and Wu (2012) overestimates some of the specimens (see the square data points in Fig. 13a). For specimens with RCLs, all the three models overestimate most of the specimens. This is reasonable as the strength of f_c' does not include the column size effect which has been found to be significant in FRP-confined compound concrete specimens (Fig. 9b). When the strength of f_{cco}' was used, both models of Lin (2016) and Wang et al. (2012a) provide conservative predictions for most of the specimens with RCLs (see the solid data points in Fig. 13b), particularly for the large-scale specimens with an RCL characteristic size ratio of 0.33-0.50. Wei and Wu's (2012) model performs reasonably well for all the specimens with and without RCLs. The above comparison indicates that the column size effect should be taken into consideration if an accurate or conservative prediction is anticipated in the practical design of FRP-confined square compound concrete columns.

Conclusions

The present paper presents the results of an experimental program aimed at clarifying the possible column size effect in FRP-confined square compound concrete containing RCLs. Three column sizes with a sectional width of 200, 300, and 400 mm were tested. The columns of different sizes had the same effective FRP confinement stiffness and thus the column size effect could be identified. Besides, the effects of characteristic size ratio of RCLs and FRP confinement level (i.e., FRP tube thickness) on the stress-strain behavior of FRP-confined compound concrete were investigated. The following conclusions may be drawn based on the present study:

1. For unconfined concrete specimens, the presence of RCLs obviously reduced the compressive strength of compound concrete and larger RCLs (with the same RCL mix ratio) led to a more negative effect on the compressive strength of compound concrete; the axial strain at peak stress of compound concrete was generally smaller than that of normal concrete without RCLs.
2. For the tested FRP-confined compound concrete specimens, the compressive strengths were remarkably lower than those of the corresponding FRP-confined normal concrete specimens without RCLs; the post-peak axial stress reduced much more gradually in specimens containing RCLs.
3. The column size had only a small influence on the stress-strain curve of unconfined concrete

specimens without RCLs; however, for the unconfined specimens containing RCLs, the stress-strain curves of the specimens of different column sizes were significantly different from each other in terms of both the compressive strength and the stress-strain curve (both the strength and the initial axial stiffness decreased dramatically with an increase in the column size).

4. The column size effect on compressive strength was not obvious in FRP-confined normal concrete specimens without RCLs while it became much more obvious for FRP-confined compound concrete column specimens with RCL characteristic size ratios of 0.25-0.33. After the effects of column size and RCLs on the compressive strength of unconfined concrete were eliminated, the size effect of FRP-confined compound concrete specimens became less obvious.
5. The negative effect of RCLs (in the case that the strength of RCLs is smaller than that of FC as in the present study) on the compressive strength should be taken into consideration in making predictions for FRP-confined compound concrete.
6. When the column size effect was not considered but the effect of RCLs was considered (i.e., when the strength of unconfined compound concrete obtained from small-scale specimens, f_c', was used), all the three models (Wang et al. 2012a; Wei and Wu 2012; Lin 2016) overestimated most of the FRP-confined compound concrete specimens, indicating that the column size effect needs be taken into consideration if an accurate or conservative prediction is anticipated in the practical design of FRP-confined square compound concrete columns.
7. It should be noted that the above conclusions on column size effect may only be applicable to FRP-confined square compound concrete columns similar to those tested in the present study (i.e., with sectional widths from 200 to 400 mm and with a softening behavior). More experimental studies with wider ranges of column parameters, including specimen sizes, FRP confinement stiffnesses, and concrete strengths, are needed for a more comprehensive investigation on the column size effect. In addition, more specimens and more than one repeated specimen should be tested for each column configuration in future studies.

Data Availability Statement

All data, models, or code that support the findings of this study are available from the corresponding author upon reasonable request.

Acknowledgements

The authors are grateful for the financial support received from the National Natural Science Foundation of China (Project Nos.: 51678161, 51978281, and 52008361), Guangdong Provincial Key Laboratory of Modern Civil Engineering Technology (Project No.:

2021B1212040003), and the Research Grants Council of the Hong Kong Special Administrative Region (Project No: T22-502/18-R).

References

Ajdukiewicz, A., and Kliszczewicz, A. (2002). "Influence of recycled aggregates on mechanical properties of HS/HPC." *Cement and Concrete Composites*, 24(2), 269-279.

ASTM C469 (2014). *Standard Test Method for Static Modulus of Elasticity and Poisson's Ratio of Concrete in Compression*. ASTM International, West Conshohocken, Pennsylvania, USA.

ASTM D3039 (2017). *Standard Test Method for Tensile Properties of Ploymer Matrix Composite Materials*. ASTM International, West Conshohocken, Pennsylvania, USA.

Bažant, Z. P., and Kwon, Y. W. (1994). "Failure of slender and stocky reinforced-concrete columns - tests of size effect." *Materials and Structures*, 27(166), 79-90.

Bažant, Z. P. (2000). "Size effect." *International Journal of Solids and Structures*, 37(1-2), 69-80.

CECS (2007). *Technical Specification for Testing Concrete Strength with Drilled Core*. China Architecture & Building Press.

Chen, G. M., J. J. Zhang, Y. F. Wu, G. Lin and T. Jiang. (2021). "Stress–strain behavior of FRP-confined recycled aggregate concrete in square columns of different sizes." *Journal of Composites for Construction*, ASCE, 25(5), 04021040.

De Luca, A., Nardone, F., Matta, F., Nanni, A., Lignola, G. P., and Prota, A. (2011). "Structural evaluation of full-scale FRP-confined reinforced concrete columns." *Journal of Composites for Construction*, ASCE, 15(1), 112-123.

Deresa, S. T., Xu, J., Demartino, C., Heo, Y., Li, Z., and Xiao, Y. (2020). "A review of experimental results on structural performance of reinforced recycled aggregate concrete beams and columns." *Advances in Structural Engineering*, 23(15), 3351-3369.

Fanaradelli, T., Rousakis, T., and Karabinis, A. (2019). "Reinforced concrete columns of square and rectangular section, confined with FRP–Prediction of stress and strain at failure." *Composites Part B: Engineering*, 174, 107046.

JGJ 52 (2006). *Standard for Technical Requirements and Tests Method of Sand and Crushed Stone (or Gravel) for Ordinary Concrete*. Ministry of Housing and Urban-Rural Development of People's Republic of China, China

Jiang, J., Li, P., and Nisticò, N. (2019). "Local and global prediction on stress-strain behavior of FRP-confined square concrete sections." *Composite Structures*, 226, 111205.

JTG E42 (2005). *Test Method of Aggregate for Highway Engineering*. Ministry of Transport of the People's Republic of China, China.

Kou, S. C., and Poon, C. S. (2015). "Effect of the quality of parent concrete on the properties of high performance recycled aggregate concrete." *Construction and Building Materials*, 77, 501-508.

Lam, L., and Teng, J. G. (2003). "Design-oriented stress–strain model for FRP-confined concrete." *Construction and Building Materials*, 17(6-7), 471-489.

Li, P., Sui, L., Xing, F., Li, M., Zhou, Y., and Wu, Y.-F. (2019). "Stress–strain relation of FRP-confined predamaged concrete prisms with square sections of different corner radii subjected to monotonic axial compression." *Journal of Composites for Construction*, ASCE, 23(2), 04019001.

Li, W., Xiao, J., Shi, C., and Poon, C. S. (2015). "Structural behaviour of composite members with recycled aggregate concrete—an overview." *Advances in Structural Engineering*, 18(6), 919-938.

Lim, J. C., and Ozbakkaloglu, T. (2014). "Design model for FRP-confined normal-and high-strength concrete square and rectangular columns." *Magazine of Concrete Research*, 66(20), 1020-1035.

Lin, G. (2016). *Seismic Performance of FRP-confined RC Columns: Stress-strain models and Numerical Simulation*. Ph.D. thesis, Department of Civil and Environmental Engineering, The Hong Kong Polytechnic University.

Lin, G., Yu, T., and Teng, J. G. (2016). "Design-oriented stress–strain model for concrete under combined FRP-steel confinement." *Journal of Composites for Construction*, ASCE, 20(4), 04015084.

Lin, G., and Teng, J. G. (2020). "Advanced stress-strain model for FRP-confined concrete in square columns." *Composites Part B: Engineering*, 197, 108149.

Matthys, S., Toutanji, H., Audenaert, K., and Taerwe, L. (2005). "Axial load behavior of large-scale columns confined with fiber-reinforced polymer composites." *ACI Structural Journal*, 102(2), 258-267.

Medina, C., Zhu, W. Z., Howind, T., Sanchez De Rojas, M. I., and Frias, M. (2015). "Influence of interfacial transition zone on engineering properties of the concrete manufactured with recycled ceramic aggregate." *Journal of Civil Engineering and Management*, 21(1), 83-93.

Park, R. (1988) "Ductility evaluation from laboratory and analytical testing." *Proceedings of the 9th World Conference on Earthquake Engineering, Tokyo-Kyoto, Japan*, 605-616.

Poon, C. S., Shui, Z. H., and Lam, L. (2004). "Effect of microstructure of ITZ on compressive strength of concrete prepared with recycled aggregates." *Construction and Building Materials*, 18(6), 461-468.

Poon, C. S., and Chan, D. X. (2006a). "Feasible use of recycled concrete aggregates and crushed clay brick as unbound road sub-base." *Construction and Building Materials*, 20(8), 578-585.

Poon, C. S., and Chan, D. X. (2006b). "Paving blocks made with recycled concrete aggregate and crushed clay brick." *Construction and Building Materials*, 20(8), 569-577.

Rahal, K. (2007). "Mechanical properties of concrete with recycled coarse aggregate." *Building* *and Environment*, 42(1), 407-15.

Rao, M. C., Bhattacharyya, S. K., and Barai, S. V. (2011). “Influence of field recycled coarse aggregate on properties of concrete.” *Materials and Structures*, 44, 205–20.

Rocca, S. (2007). *Experimental and Analytical Evaluation of FRP-confined Large Size Reinforced Concrete Columns*. Ph.D. thesis, Civil Engineering, University of Missouri-Rolla.

Teng, J. G., Zhao, J. L., Yu, T., Li, L. J., and Guo, Y. C. (2016). “Behavior of FRP-confined compound concrete containing recycled concrete lumps.” *Journal of Composites for Construction*, ASCE, 20(1), 04015038.

Topcu, I. B., and Sengel., S. (2004). “Properties of concretes produced with waste concrete aggregate.” *Cement and Concrete Research*, 34(8).

Wang, D. Y., Wang, Z. Y., Smith, S. T., and Yu, T. (2016). “Size effect on axial stress-strain behavior of CFRP-confined square concrete columns.” *Construction and Building Materials*, 118, 116-126.

Wang, Z., Wang, D., Smith, S. T., and Lu, D. (2012a). “CFRP-confined square RC columns. II: Cyclic axial compression stress-strain model.” *Journal of Composites for Construction*, ASCE, 16(2), 161-170.

Wang, Z. Y., Wang, D. Y., Smith, S. T., and Lu, D. G. (2012b). “CFRP-confined square RC columns. I: Experimental investigation.” *Journal of Composites for Construction*, ASCE, 16(2), 150-160.

Wei, Y. Y., and Wu, Y. F. (2012). “Unified stress-strain model of concrete for FRP-confined columns.” *Construction and Building Materials*, 26(1), 381-392.

Wu, B., Liu, Q. X., Liu, W., and Xu, Z. (2008). “Primary study on recycledconcrete-segment filled steel tubular members.” *Earthquake Resistant Engineering Retrofitting*, 30(4), 120-124.

Wu, B., Xu, Z., Ma, Z. J., Liu, Q. X., and Liu, W. (2011a). “Behavior of reinforced concrete beams filled with demolished concrete lumps.” *Structural Engineering and Mechanics*, 40(3), 411-429.

Wu, B., Zhao, X. Y., Liu, W., Liu, Q. X., and Xu, Z. (2011b). “Axial strengths of concrete stub columns filled with demolished concrete segments/lumps.” *Advanced Science Letters*, 4(8-10), 2719-2726.

Wu, B., Zhao, X. Y., and Zhang, J. S. (2012). “Cyclic behavior of thin-walled square steel tubular columns filled with demolished concrete lumps and fresh concrete.” *Journal of Constructional Steel Research*, 77, 69-81.

Wu, B., Liu, C. H., and Yang, Y. (2013a). “Size effect on compressive behaviours of normal-strength concrete cubes made from demolished concrete blocks and fresh concrete.” *Magazine of Concrete Research*, 65(19), 1155-1167.

Wu, B., Zhao, X. Y., Zhang, J. S., and Yang, Y. (2013b). “Cyclic testing of thin-walled circular steel tubular columns filled with demolished concrete blocks and fresh concrete.” *Thin-*

Walled Structures, 66, 50-61.

Wu, B., Liu, C. H., and Wu, Y. P. (2014). “Compressive behaviors of cylindrical concrete specimens made of demolished concrete blocks and fresh concrete.” *Construction and Building Materials*, 53, 118-130.

Wu, B., Zhang, S. Y., and Yang, Y. (2015). “Compressive behaviors of cubes and cylinders made of normal-strength demolished concrete blocks and high-strength fresh concrete.” *Construction and Building Materials*, 78, 342-353.

Wu, B., Zhang, Q., and Chen, G. M. (2018). “Compressive behavior of thin-walled circular steel tubular columns filled with steel stirrup-reinforced compound concrete.” *Engineering Structures*, 170, 178-195.

Xiao, J. Z., and Falkner, H. (2007). “Bond behaviour between recycled aggregate concrete and steel rebars.” *Construction and Building Materials*, 21(2), 395-401.

Xiao, J. Z., Li., J. B., and Zhang, C. (2005). “Mechanical properties of recycled aggregate concrete under uniaxial loading.” *Cement and Concrete Research* , 35(6), 1187-1194.

Xiao, J. Z., Li, L., Tam, V. W. Y., and Li, H. (2014). “The state of the art regarding the long-term properties of recycled aggregate concrete.” *Structural Concrete*, 15(1), 3-12.

Xie, P., Lin, G., Teng, J. G., and Jiang, T. (2020). “Modelling of concrete-filled filament-wound FRP confining tubes considering nonlinear biaxial tube behavior.” *Engineering Structures*, 218, 110762.

Zeng, J. J., Lin, G., Teng, J. G., and Li, L. J. (2018). “Behavior-of large-scale FRP-confined rectangular RC columns under axial compression.” *Engineering Structures*, 174, 629-645.

Zhang, B., Teng, J. G., and Yu, T. (2017). “Compressive behavior of double-skin tubular columns with high-strength concrete and a filament-wound FRP tube.” *Journal of Composites for Construction*, ASCE, 21(5), 04017029.

Zhao, J. L., Xu, C. H., Sun, L. Z., and Wu, D. Y. (2020). “Behaviour of FRP-confined compound concrete–filled circular thin steel tubes under axial compression.” *Advances in Structural Engineering*, 23(9), 1772-1784.

Zhao, X. Y., Wu, B., and Wang, L. (2016). “Structural response of thin-walled circular steel tubular columns filled with demolished concrete lumps and fresh concrete.” *Construction and Building Materials*, 129, 216-242.

Zhou, J. K., Lin, G., and Teng, J. G. (2021a). “Stress-strain behavior of FRP-confined concrete containing recycled concrete lumps.” *Construction and Building Materials*, 267, 120915.

Zhou, J. K., Lin, G., and Teng, J. G. (2021b). “Compound concrete-filled FRP tubular columns under cyclic axial compression.” *Composite Structures*, 275, 114329.

Zhu, J. Y., Lin, G., Teng, J. G., Chan, T. M., Zeng, J. J., and Li, L. J. (2020). “FRP-confined square concrete columns with section curvilinearization under axial compression.” *Journal of Composites for Construction*, ASCE, 24(2), 04020004.

Table 1

Specimen details.

Group	Specimen	b (mm)	H (mm)	r_c (mm)	n_f	d (mm)	β (d/b)	η (%)
Group 1	S200L0	200	600	30	0	0	0	0
	S200L2	200	600	30	2	0	0	0
	S200L0G1	200	600	30	0	50-67	0.25-0.33	33
	S200L2G1	200	600	30	2	50-67	0.25-0.33	33
	S200L0G2	200	600	30	0	67-100	0.33-0.5	33
	S200L1G2	200	600	30	1	67-100	0.33-0.5	33
	S200L2G2	200	600	30	2	67-100	0.33-0.5	33
Group 2	S300L0	300	900	45	0	0	0	0
	S300L3	300	900	45	3	0	0	0
	S300L0G1	300	900	45	0	75-100	0.25-0.33	33
	S300L3G1	300	900	45	3	75-100	0.25-0.33	33
	S300L0G2	300	900	45	0	100-150	0.33-0.5	33
	S300L3G2	300	900	45	3	100-150	0.33-0.5	33
Group 3	S400L0	400	1200	60	0	0	0	0
	S400L4	400	1200	60	4	0	0	0
	S400L0G1	400	1200	60	0	100-133	0.25-0.33	33
	S400L4G1	400	1200	60	4	100-133	0.25-0.33	33
	S400L0G2	400	1200	60	0	133-200	0.33-0.5	33
	S400L2G2	400	1200	60	2	133-200	0.33-0.5	33
	S400L4G2	400	1200	60	4	133-200	0.33-0.5	33

Note: b = sectional width; H = specimen height; r_c = corner radius; n_f = number of FRP layers; d = characteristic size of RCLs; β = RCL characteristic size ratio; η = RCL mix ratio.

Table 2

Material properties of GFRP tube.

Specimen	Nominal thickness t_f (mm)	Tensile strength f_f (MPa)			Rupture strain ε_f (%)			Elastic modulus E_f (GPa)		
		Test	Ave.	Std.	Test	Ave.	Std.	Test	Ave.	Std.
1	0.36	1442	1410	103	1.89	1.87	0.10	76	75	1.64
2		1294			1.76			73		
3		1493			1.96			76		

Note: Ave. = Average; Std. = Standard Deviation.

Table 3

Key test results.

Group	Specimen	r_c (mm)	t_f (mm)	E_f (GPa)	f'_{cc} (MPa)	f'_{cco} (MPa)	f'_c (MPa)	f'_{cc}/f'_{cco}	$f'_{cu,r}$ (MPa)	ε_{cc} (%)	$\varepsilon_{cc}/\varepsilon_{cco}$	$\varepsilon_{cu,r}$ (%)	ε_y (%)	ε_{cu} (%)	DI
G1	S200L0	30	-	-	67.5			1.00	-	0.209	-	-	0.162	-	-
	S200L2	30	0.72	75	75.8	67.5	67.5	1.12	50.7	0.240	1.15	0.594	0.209	0.246	1.18
	S200L0G1	30	-	-	48.6			1.00	-	0.165	-	-	0.133	-	-
	S200L2G1	30	0.72	75	59.2	48.6	48.6	1.22	46.7	0.202	1.22	0.516	0.165	0.346	2.10
	S200L0G2	30	-	-	45.1			1.00	-	0.150	-	-	0.124	-	-
	S200L1G2	30	0.36	75	46.4	45.1	45.1	1.03	33.8	0.179	1.19	0.456	0.144	0.312	2.17
	S200L2G2	30	0.72	75	49.6	45.1	45.1	1.10	49.2	0.494	3.29	0.502	0.157	0.502*	3.19
G2	S300L0	45	-	-	64.0			1.00	-	0.182	-	-	0.163	-	-
	S300L3	45	1.08	75	70.8	64.0	67.5	1.11	44.4	0.281	1.54	0.520	0.197	0.343	1.74
	S300L0G1	45	-	-	43.8			1.00	-	0.145	-	-	0.123	-	-
	S300L3G1	45	1.08	75	55.5	43.8	48.6	1.27	48.5	0.204	1.41	0.469	0.156	0.469*	3.01
	S300L0G2	45	-	-	41.3			1.00	-	0.151	-	-	0.119	-	-
	S300L3G2	45	1.08	75	46.7	41.3	45.1	1.13	43.9	0.201	1.33	0.401	0.149	0.401*	2.69
G3	S400L0	60	-	-	64.5			1.00	-	0.176	-	-	0.163	-	-
	S400L4	60	1.44	75	74.6	64.5	67.5	1.16	43.7	0.200	1.14	0.482	0.184	0.208	1.13
	S400L0G1	60	-	-	41.1			1.00	-	0.161	-	-	0.132	-	-
	S400L4G1	60	1.44	75	47.4	41.1	48.6	1.15	44.0	0.219	1.36	0.467	0.155	0.467*	3.02
	S400L0G2	60	-	-	36.3			1.00	-	0.153	-	-	0.123	-	-
	S400L2G2	60	0.72	75	44.5	36.3	45.1	1.23	27.6	0.158	1.03	0.393	0.140	0.207	1.48
	S400L4G2	60	1.44	75	48.2	36.3	45.1	1.33	43.1	0.183	1.20	0.323	0.156	0.323*	2.07

Notes: f'_{cc} and ε_{cc} = peak axial stress and corresponding axial strain; $f'_{cu,r}$ and $\varepsilon_{cu,r}$ = axial stress and axial strain at FRP rupture; f'_{cco} and ε_{cco} = compressive strength and corresponding axial strain of the control unconfined concrete specimen; f'_c = compressive strength of unconfined compound concrete obtained from small-scale unconfined specimens; ε_{cu} = ultimate axial strain corresponding to an 15% decay in axial stress after the peak or the rupture of FRP tube, whichever occurs first; ε_y = yield axial strain; DI = ductility index ($\varepsilon_{cu}/\varepsilon_y$); * FRP rupture occurred before an 15% decay in axial stress was reached.

Table 4
FRP hoop strains in the test FRP-confined specimens.

Specimen	$\varepsilon_{h,f}$ (%)		$\varepsilon_{h,t}$ (%)		$\varepsilon_{h,c}$ (%)		$\varepsilon_{h,\,max}$ (%)
	At f'_{cc}	At $f'_{cu,r}$	At f'_{cc}	At $f'_{cu,r}$	At f'_{cc}	At $f'_{cu,r}$	
S200L2	0.210	0.888	0.092	0.783	0.075	0.703	1.149 (SG18)
S200L2G1	0.142	1.064	0.094	0.790	0.086	0.859	1.288 (SG6)
S200L1G2	0.142	0.805	0.115	0.778	0.098	0.818	0.932 (SG11)
S200L2G2	0.760	0.772	0.656	0.688	0.667	0.705	1.027 (SG6)
S300L3	0.077	1.028	0.047	0.805	0.057	0.743	1.043 (SG1)
S300L3G1	0.261	1.015	0.231	0.874	0.214	0.909	1.368 (SG18)
S300L3G2	0.251	0.765	0.204	0.655	0.147	0.617	0.968 (SG13)
S400L4	0.047	0.577	0.043	0.607	0.050	0.604	0.795 (SG3)
S400L4G1	0.356	1.038	0.226	0.790	0.219	0.938	1.203 (SG18)
S400L2G2	0.085	1.190	0.080	0.845	0.067	0.798	1.260 (SG3)
S400L4G2	0.241	1.056	0.165	0.695	0.139	0.736	1.182 (SG6)

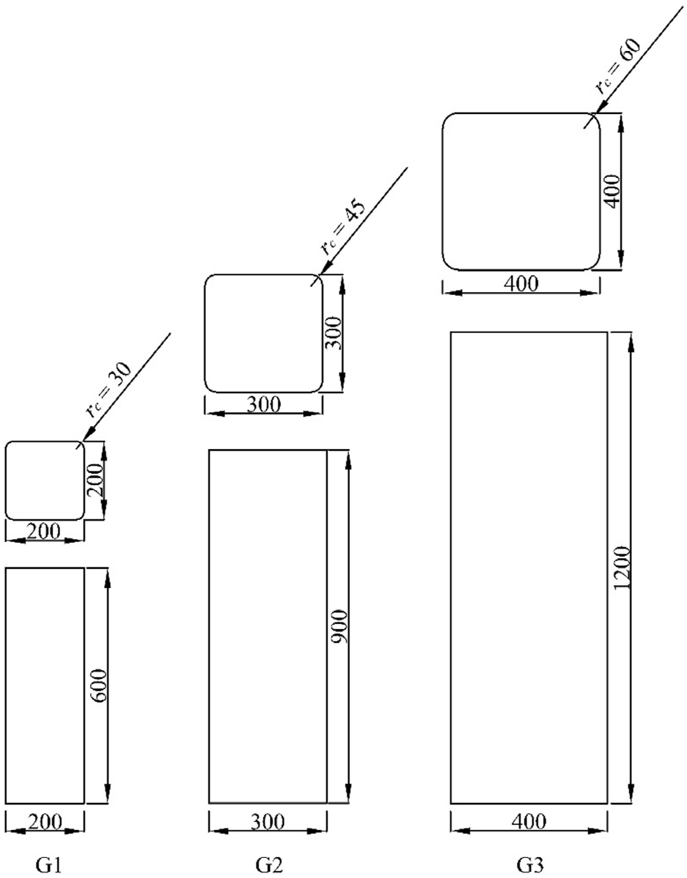

Fig. 1. Specimen dimensions (mm)

Figure 2

Click here to access/download;Figure;Figure 2.pdf

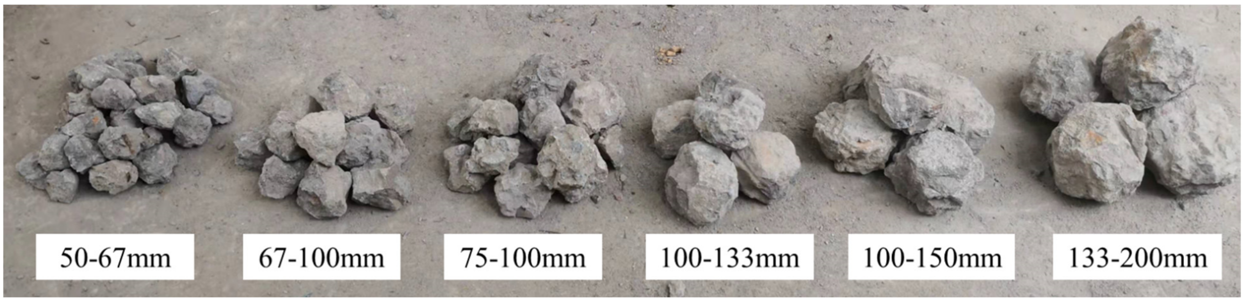

Fig. 2. RCLs of different characteristic sizes

Fig. 3. Fabrication of GFRP tubes

Figure 4

Click here to access/download;Figure;Figure 4.pdf

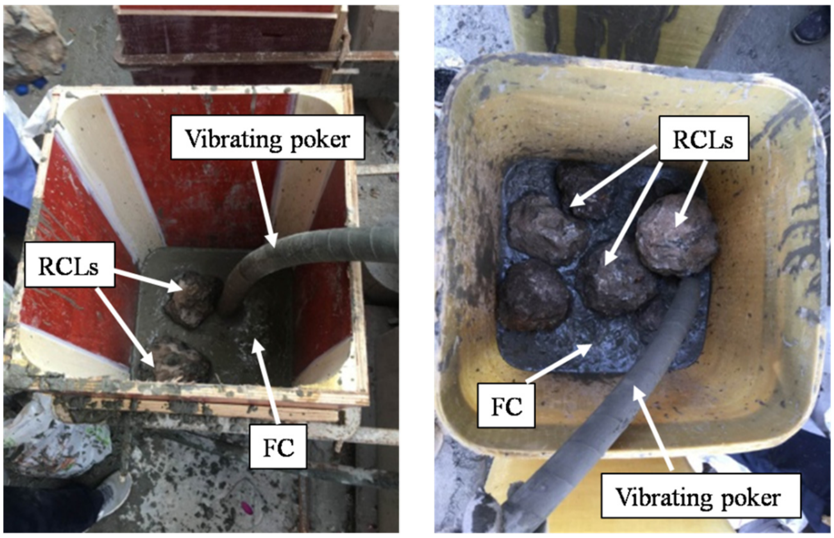

Fig. 4. Casting of compound concrete specimens

Figure 5

Click here to access/download;Figure;Figure 5.pdf

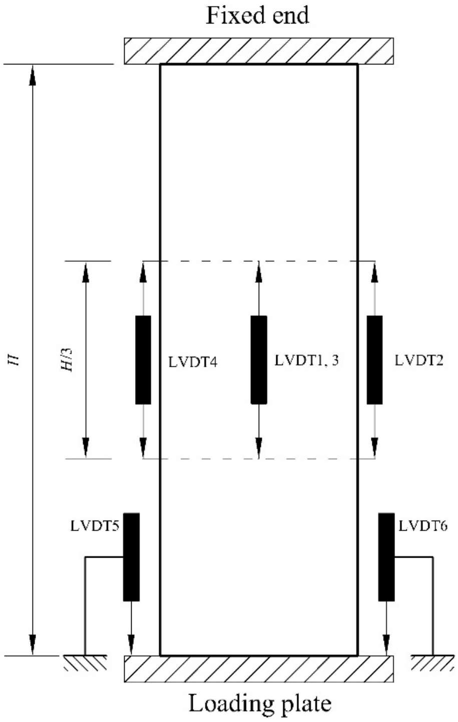

(a) Elevation

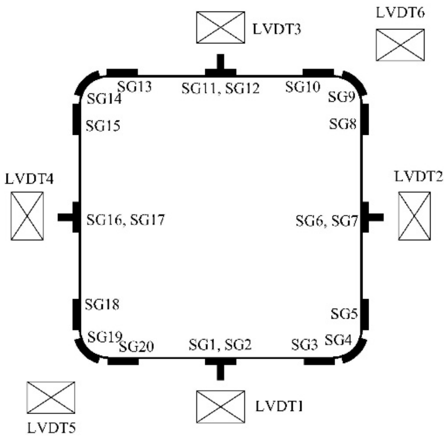

(b) LVDT and strain gauge layouts

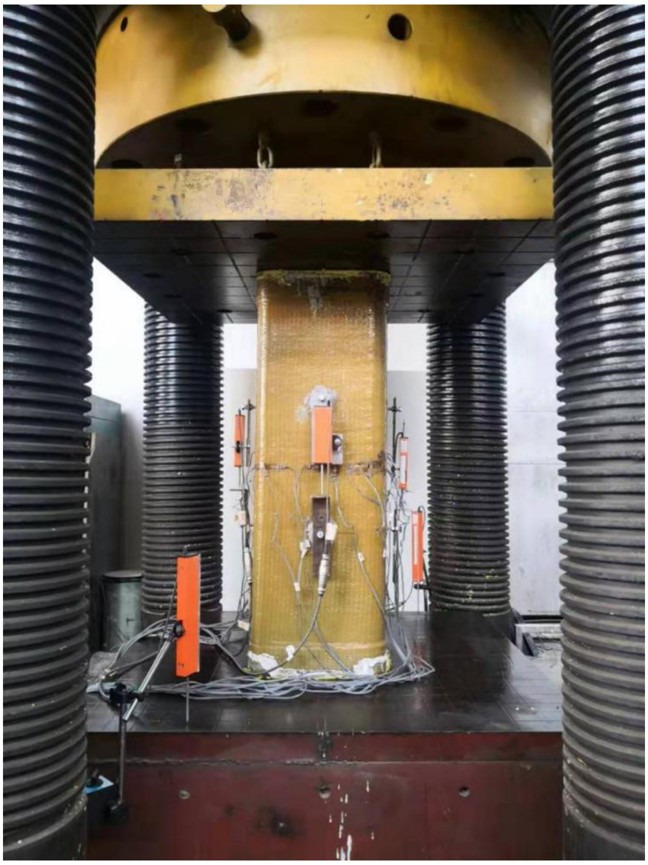

(c) Test set-up

Fig. 5. Instrumentation and test set-up

Figure 6 Click here to access/download;Figure;Figure 6.pdf

(a) Specimens in G1 group

(b) Specimens in G2 group

(c) Specimens in G3 group

Fig. 6. Failure modes

Figure 7

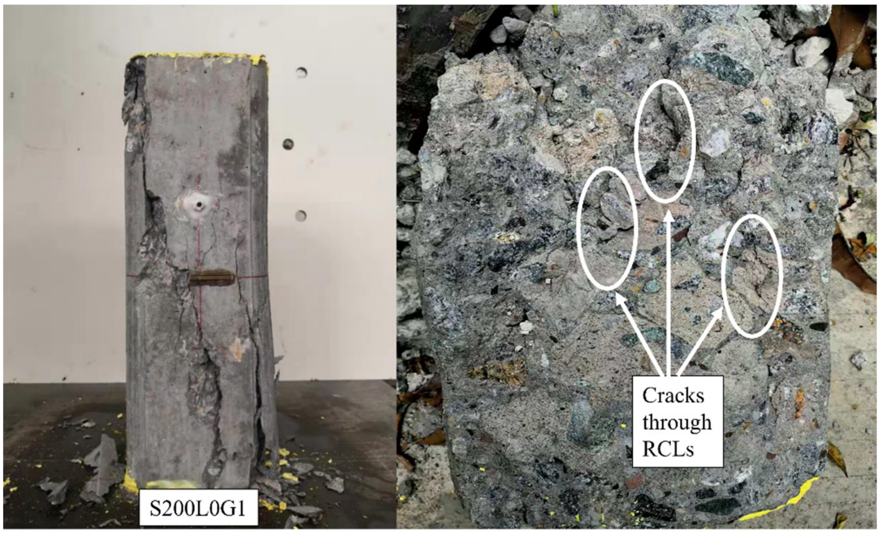

(a) S200L0G1

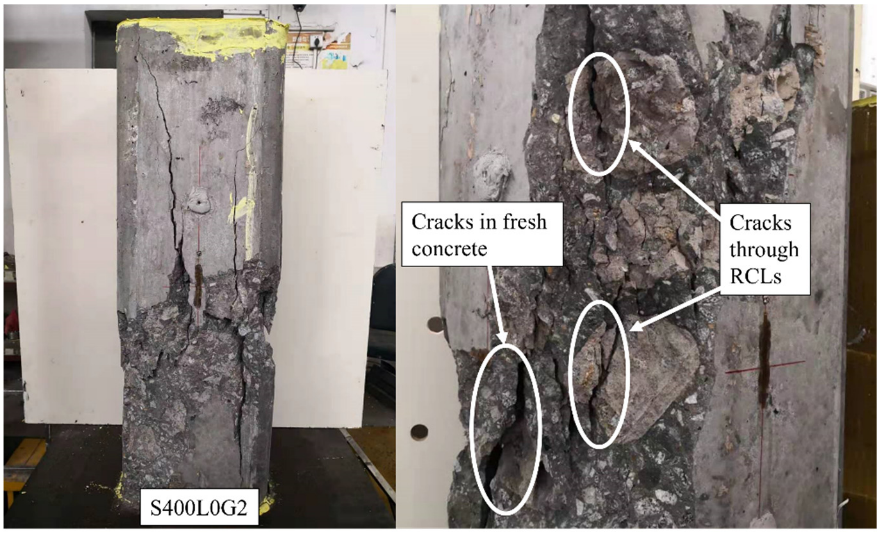

(b) S400L0G2

Fig. 7. Close-up view of unconfined specimens containing RCLs

Figure 8

Click here to access/download;Figure;Figure 8.pdf

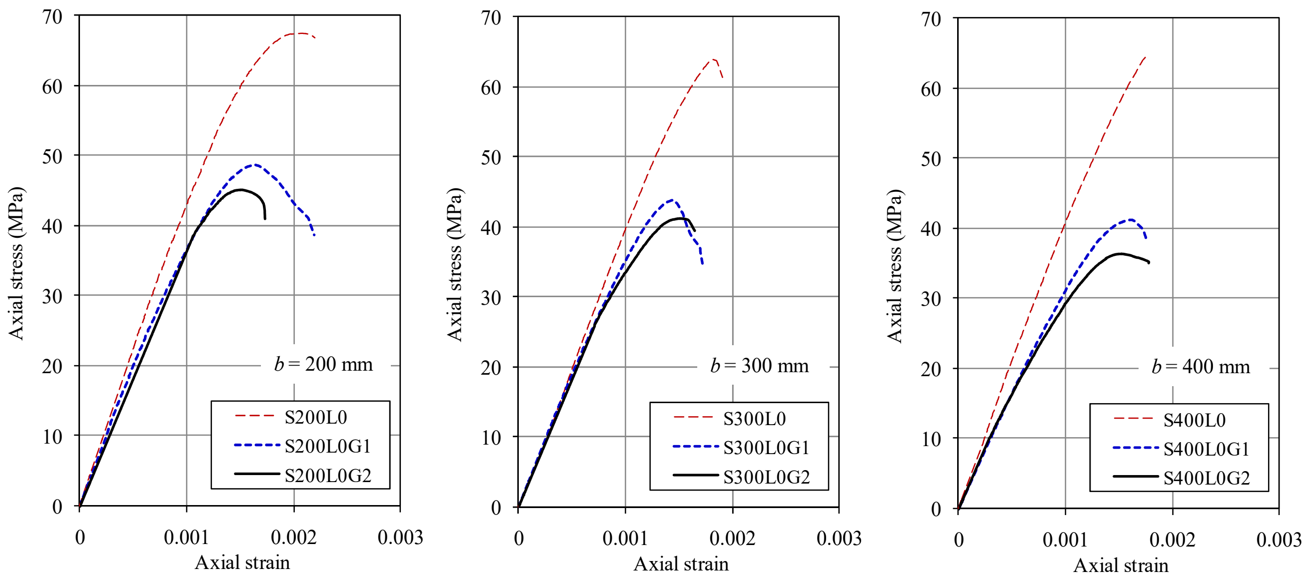

(a) Unconfined concrete specimens

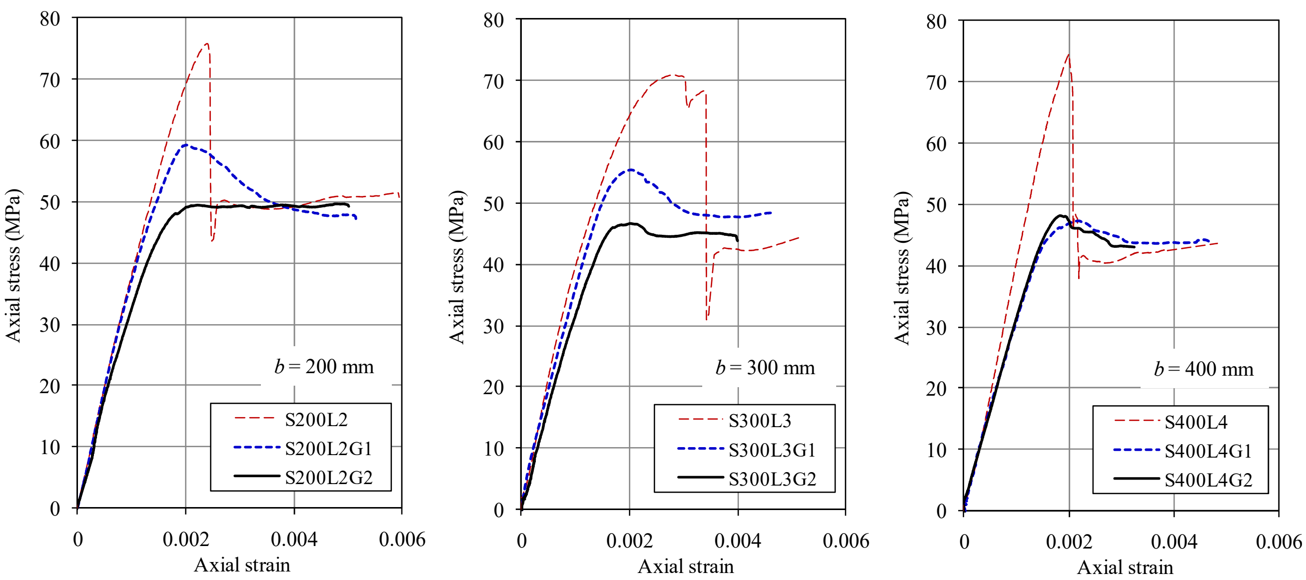

(b) FRP-confined concrete specimens

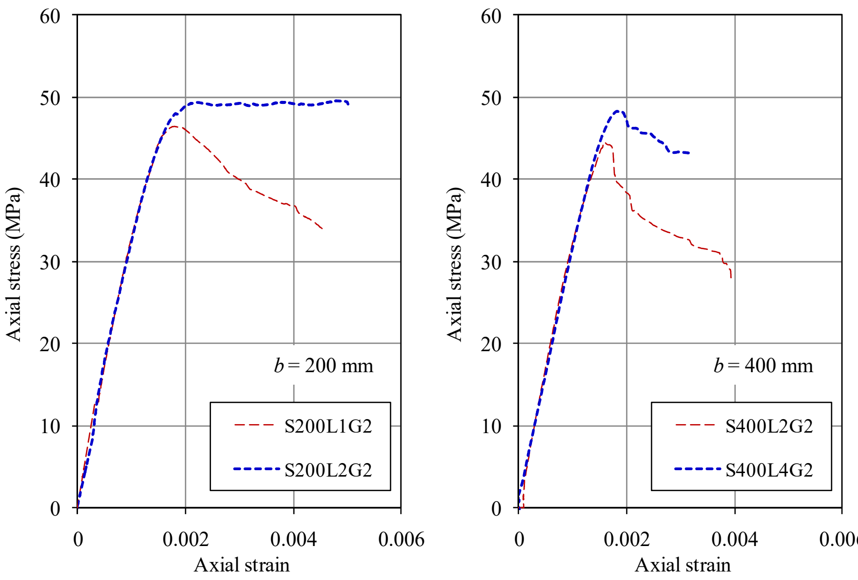

(c) FRP-confined concrete specimens with varied FRP thicknesses (β = 0.33-0.5)

Fig. 8. Axial stress-axial strain curves of concrete in the test specimens

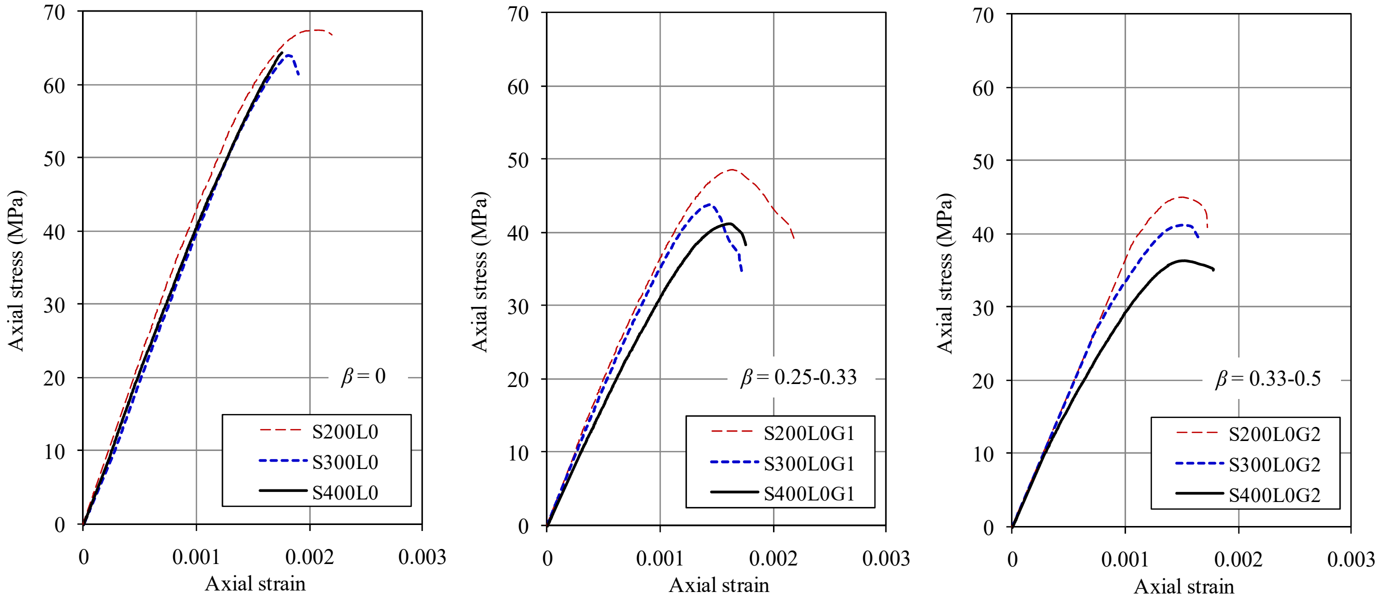

(a) Unconfined concrete specimens

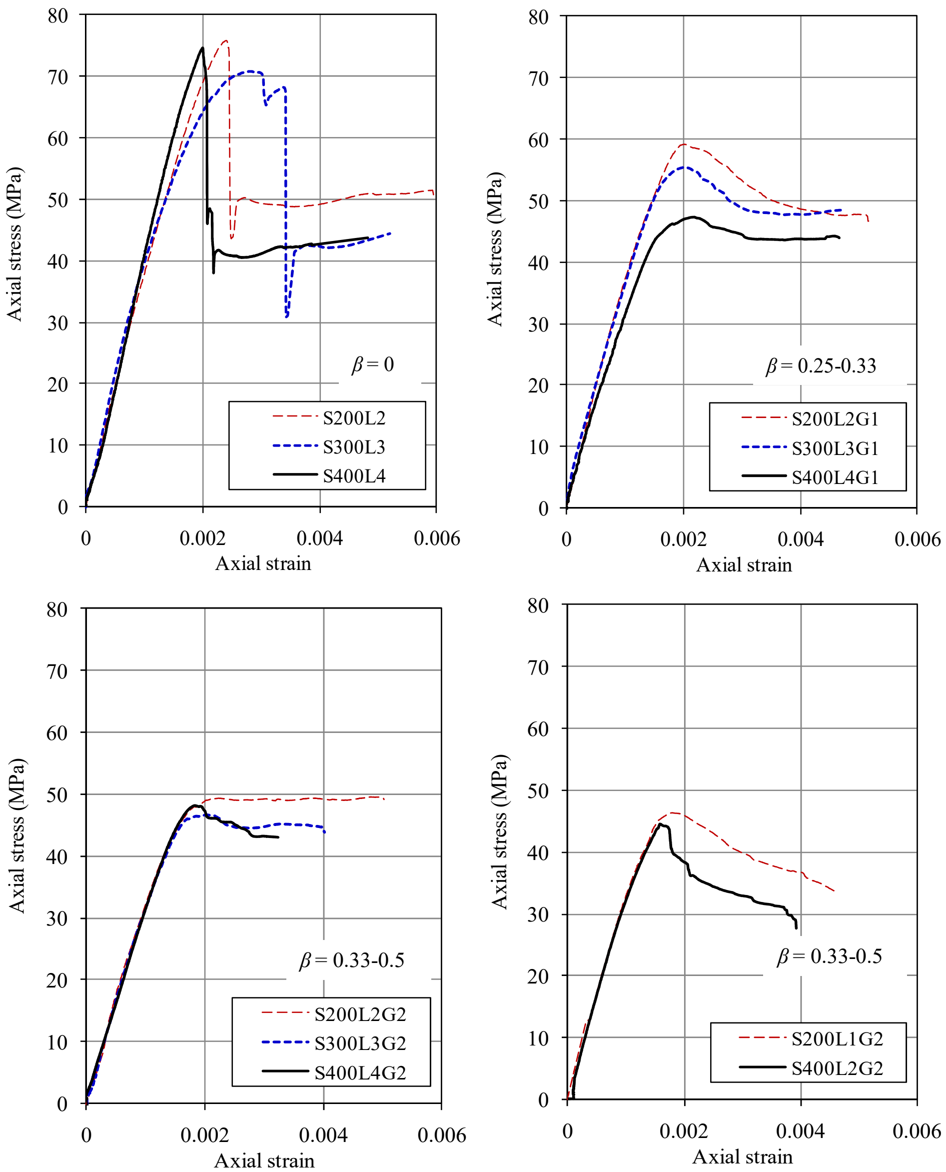

(b) FRP-confined concrete specimens

Fig. 9. Comparisons of stress-strain curves of specimens having the same confinement stiffness

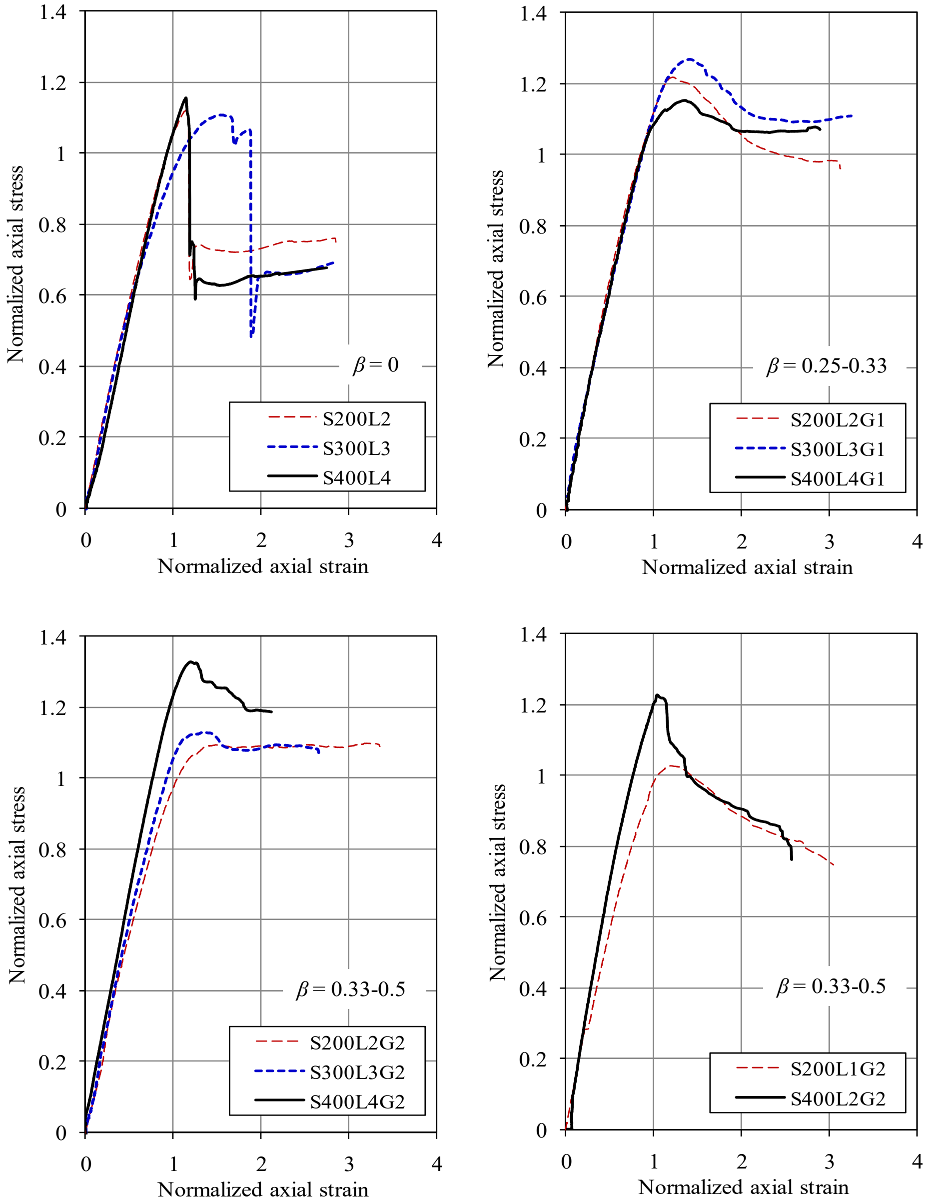

Fig. 10. Comparisons of normalized stress-strain curves of FRP-confined specimens with the same FRP confinement stiffness

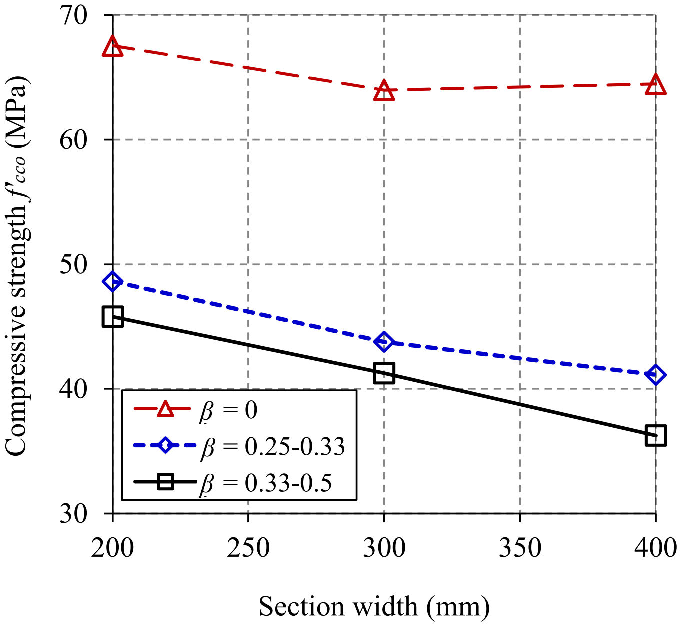

(a) Unconfined concrete specimens

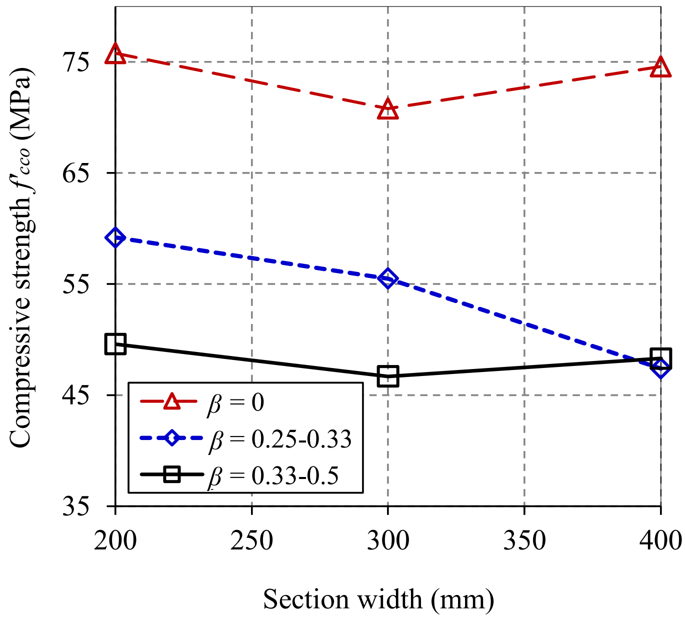

(b) FRP-confined concrete specimens

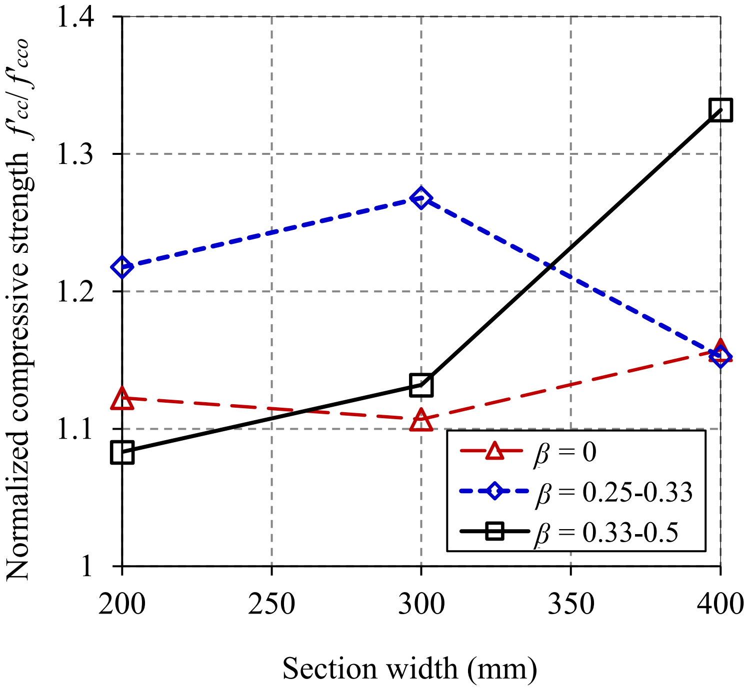

(c) Normalized compressive strength

Fig. 11. Effects of characteristic size of RCLs and column size on the compressive strength

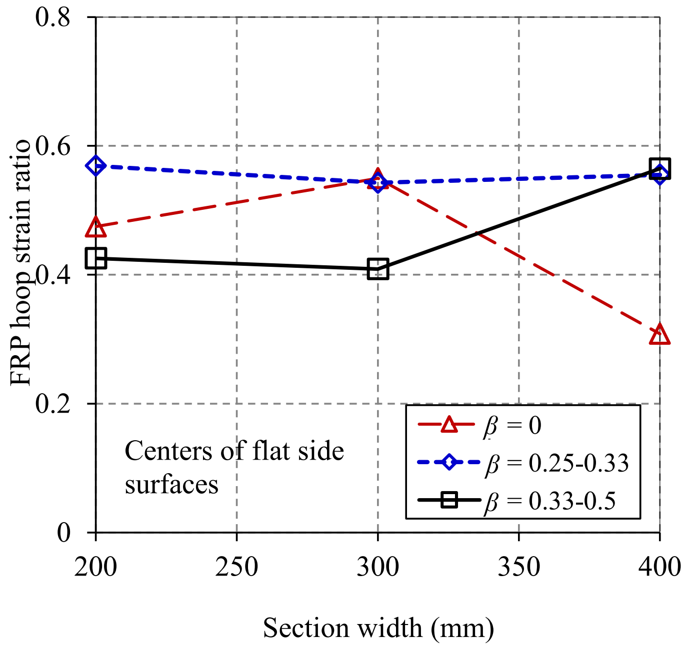

(a) Strains at centers of flat side surfaces

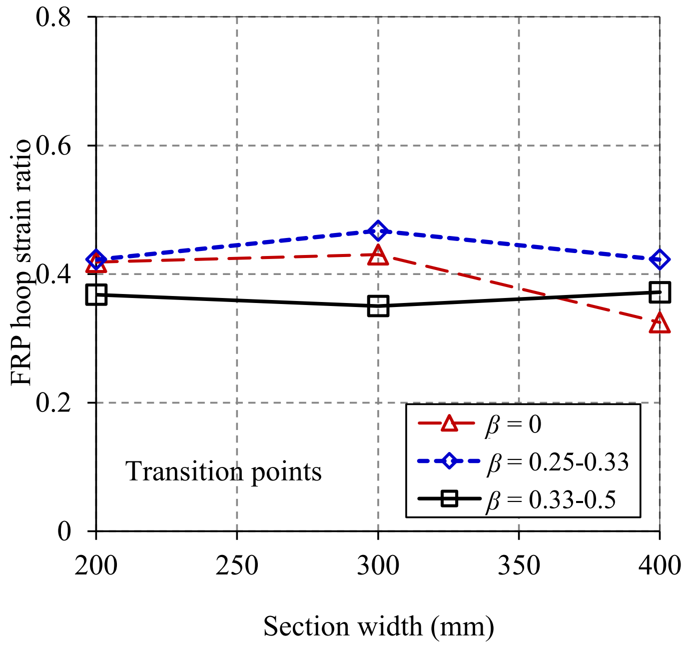

(b) Strains at transition points

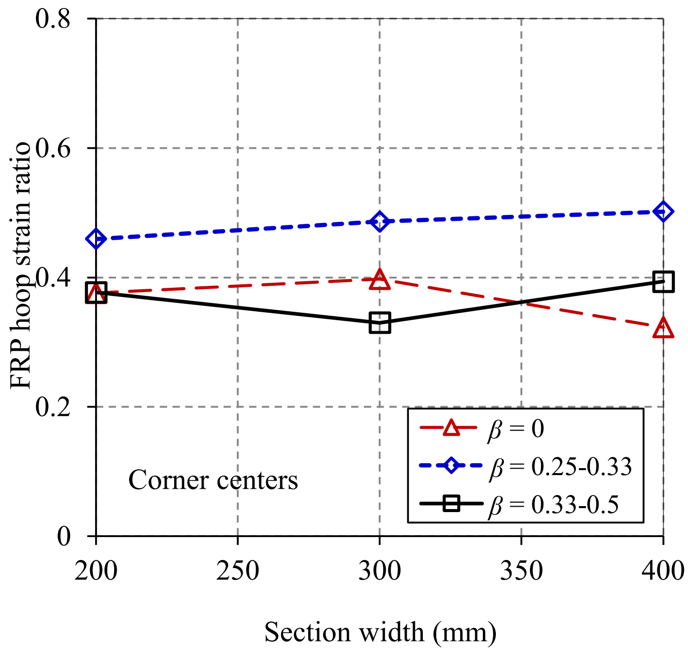

(c) Strains at the corner centers

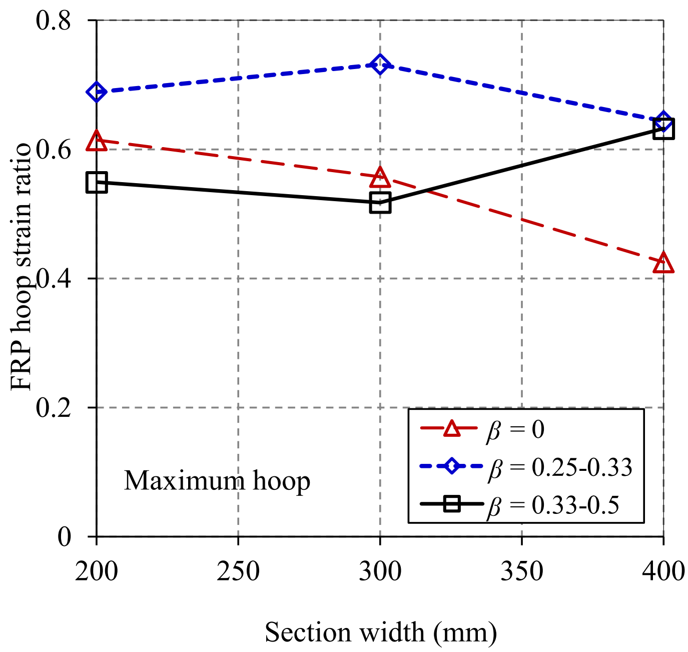

(d) Maximum hoop strains

Fig. 12. Effects of characteristic size of RCLs and column size on the FRP hoop strains

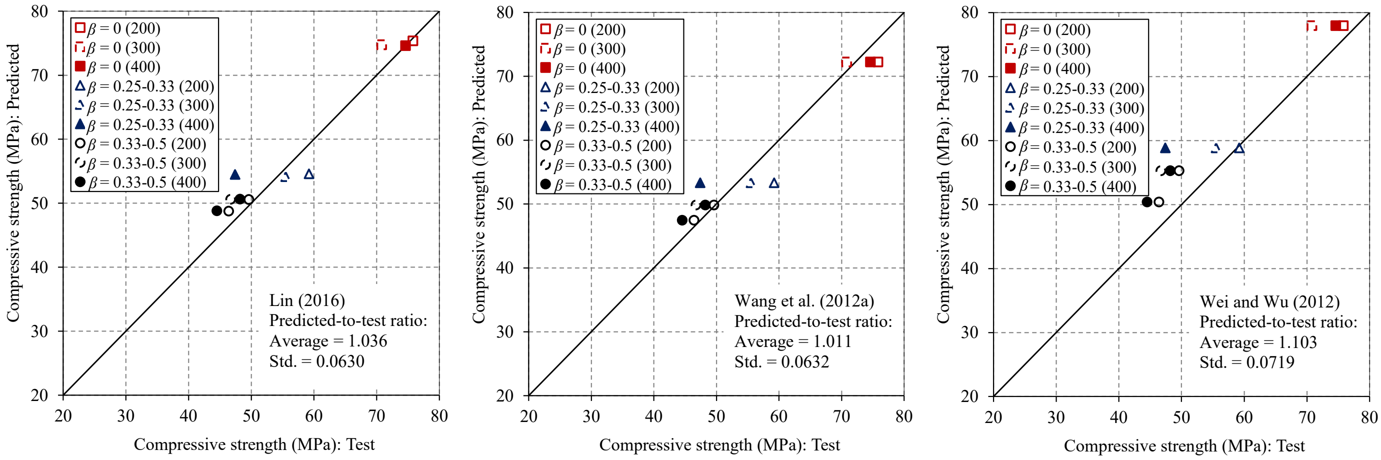

(a) Predictions based on f_c' (obtained from the corresponding small-scale unconfined compound concrete specimen)

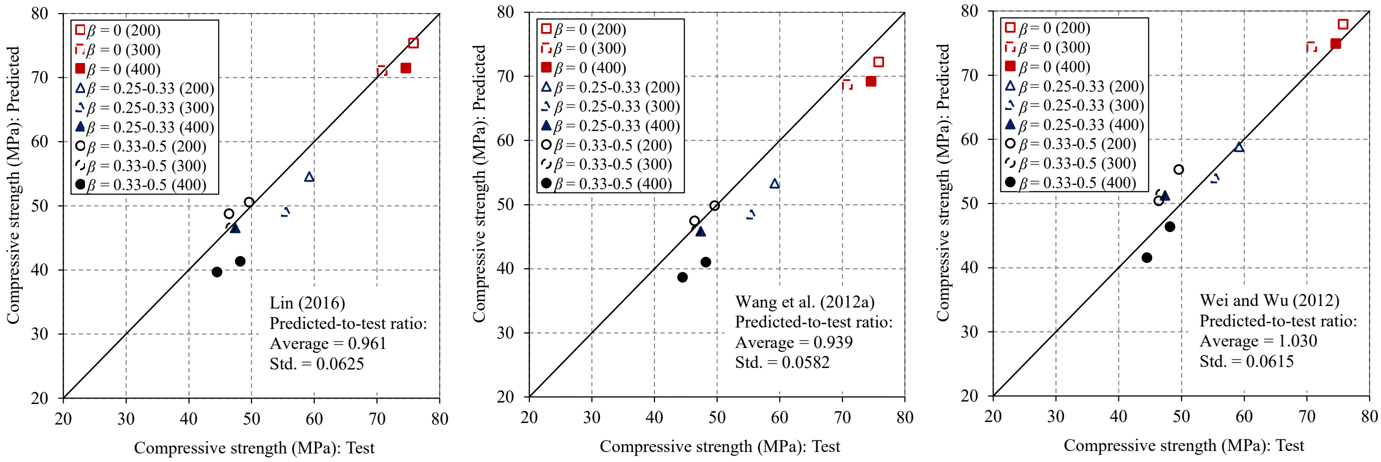

(b) Predictions based on f_{cco}' (obtained from the corresponding control unconfined compound concrete specimen)

Fig. 13 Performance of existing models in predicting the compressive strengths of test columns